Electronic Supplementary Material (ESI) for RSC Advances.

Mixed Tb/Dy coordination ladders based on tetra(carboxymethyl)thiacalix[4]arene: a new avenue towards luminescent molecular nanomagnets

A.S. Ovsyannikov,*[a] I.V. Khariushin,[b] S.E. Solovieva,[a] I.S. Antipin, [b] H. Komiya,[c] N. Marets,[c] H. Tanaka,[c] H. Ohmagari,[c] M. Hasegawa,[c] J. J. Zakrzewski,[d] S. Chorazy,[d] N. Kyritsakas,[e] M. W. Hosseini,[e] S. Ferlay*[e]

Electronic Supplementary Information

Shape analysis

HL3-Tb

Tb eight coordinated complex

OP-8 1 D8h Octagon
HPY-8 2 C7v Heptagonal pyramid
HBPY-83 D6h Hexagonal bipyramid
CU-8 4 Oh Cube
SAPR-85 D4d Square antiprism
TDD-8 6 D2d Triangular dodecahedron
JGBF-87 D2d Johnson gyrobifastigium J26
JETBPY-8 8 D3h Johnson elongated triangular bipyramid J14
JBTPR-8 9 C2v Biaugmented trigonal prism J50
BTPR-8 10 C2v Biaugmented trigonal prism
JSD-811 D2d Snub diphenoid J84
TT-8 12 Td Triakis tetrahedron
ETBPY-8 13 D3h Elongated trigonal bipyramid

Structure [ML8]	OP-8	HPY-8	HBPY-8	CU-8	SAPR-8	TDD-8	JGBF-8	JETBPY-8	JBTPR-8	BTPR-8	JSD-8	TT-8	ETBPY-8
	29.644	18.199	20.071	16.741	10.581	8.788	19.337	23.652	11.471	11.129	12.706	17.0 18	25.830

HL3-Dy

Dy eight coordinated complex

OP-8 1 D8h Octagon
HPY-8 2 C7v Heptagonal pyramid
HBPY-83 D6h Hexagonal bipyramid
CU-8 4 Oh Cube
SAPR-85 D4d Square antiprism
TDD-8 6 D2d Triangular dodecahedron
JGBF-87 D2d Johnson gyrobifastigium J26
JETBPY-8 8 D3h Johnson elongated triangular bipyramid J14
JBTPR-8 9 C2v Biaugmented trigonal prism J50
BTPR-8 10 C2v Biaugmented trigonal prism
JSD-811 D2d Snub diphenoid J84
TT-8 12 Td Triakis tetrahedron
ETBPY-8 13 D3h Elongated trigonal bipyramid

Structure [ML8]	OP-8	HPY-8	HBPY-8	CU-8	SAPR-8	TDD-8	JGBF-8	JETBPY-8	JBTPR-8	BTPR-8	JSD-8	TT-8	ETBPY-8
	29.589	18.053	19.856	16.547	10.377	8.656	19.403	23.683	11.373	10.954	12.658	16.846	25.838

Table S1: Measured cell parameters in **HL3-Tb$_{1-x}$Dy$_x$** Coordination Polymers.

	All compounds triclinic, space group P-*1*	
HL3-Tb	a = 15.0160(17) b = 15.9630(14) c = 16.7660(16)	α = 62.226(3) β = 67.513(3) γ = 79.132(4)° V = 3285.2(6)
HL3-Tb$_{0.95}$Dy$_{0.05}$	a = 15.01 b = 15.97 c = 16.76	α = 62.23 β = 67.54 γ = 79.14 V = 3284.9
HL3-Tb$_{0.67}$Dy$_{0.33}$	a = 15.00 b = 15.98 c = 16.75	α = 62.21 β = 67.56 γ = 79.2 V = 3282.7
HL3-Tb$_{0.42}$Dy$_{0.58}$	a = 15.02 b = 15.97 c = 16.74	α = 62.22 β = 67.55 γ = 79.17 V = 3283.1
HL3-Tb$_{0.20}$Dy$_{0.80}$	a = 15.01 b = 15.98 c = 16.74	α = 62.23 β = 67.55 γ = 79.19 V = 3283.3
HL3-Tb$_{0.07}$Dy$_{0.93}$	a = 15.02 b = 15.97 c = 16.75	α = 62.21 β = 67.56 γ = 79.17 V = 3285.0
HL3-Dy	a = 15.0091(17) b = 15.9798(18) c = 16.7401(18) Å	α = 62.217(5) β = 67.626(5) γ = 79.181(6) V = 3284.5(7)

EDS analysis

Samples **HL3-$Tb_{0.07}Dy_{0.93}$, HL3-$Tb_{0.20}Dy_{0.80}$, HL3-$Tb_{0.42}Dy_{0.58}$, HL3-$Tb_{0.67}Dy_{0.33}$ and HL3-$Tb_{0.95}Dy_{0.05}$** were analyzed after having been mixed with graphite matrix.

- **HL3-$Tb_{0.07}Dy_{0.93}$**

Element	Series	[at.%]	Sigma
O	K-series	5.79	0.29
S	K-series	1.55	1.45
Tb	L-series	0.01	0.01
Dy	L-series	0.14	0.15

- **HL3-$Tb_{0.20}Dy_{0.80}$**

Element	Series	[at.%]	Sigma
O	K-series	7.50	0.35
S	K-series	2.46	1,32
Tb	L-series	0.06	0.02
Dy	L-series	0.23	0.15

- **HL3-$Tb_{0.42}Dy_{0.58}$**

Element	Series	[at.%]	Sigma
O	K-series	6.21	0.29
S	K-series	1.37	1,41
Tb	L-series	0.06	0.02
Dy	L-series	0.08	0.12

- **HL3-$Tb_{0.67}Dy_{0.33}$**

Element	Series	[at.%]	Sigma
O	K-series	5.70	0.35
S	K-series	0.99	1,22
Tb	L-series	0.08	0.01
Dy	L-series	0.04	0.13

- **HL3-$Tb_{0.95}Dy_{0.05}$**

Element	Series	[at.%]	Sigma
O	K-series	9.63	0.42
S	K-series	2.76	1,27
Tb	L-series	0.32	0.01
Dy	L-series	0.02	0.15

Excitation spectra

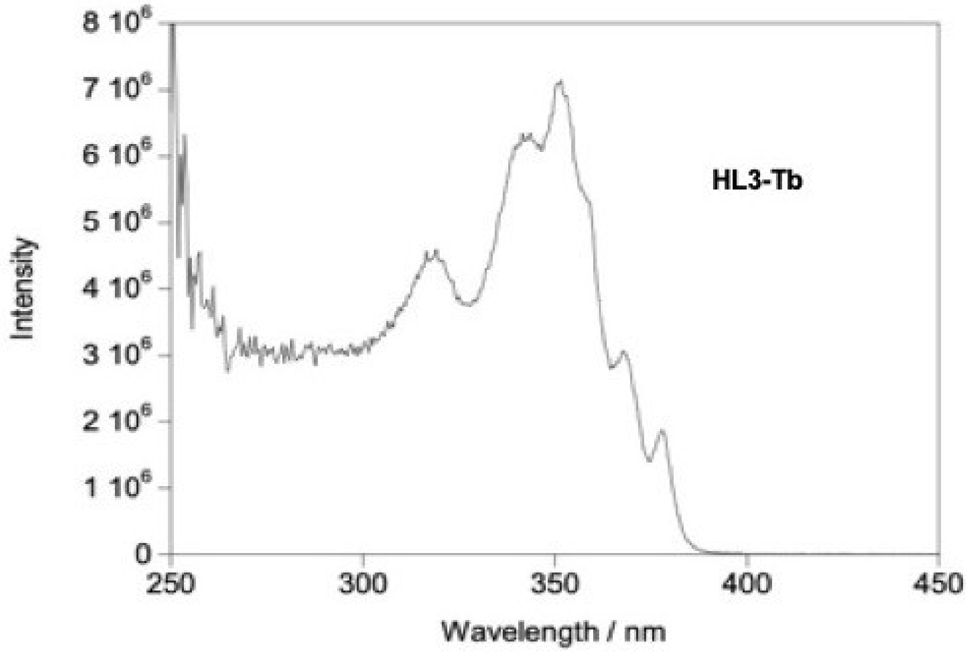

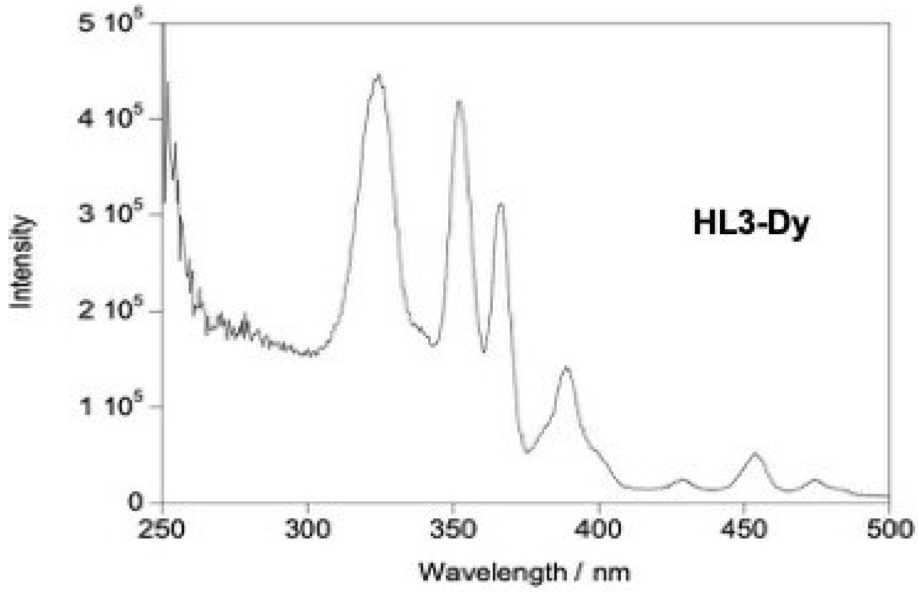

Figure S1: Excitation spectra of **HL3-Tb** (λ_{em} = 534 nm) (top) and **HL3-Dy** (λ_{em} = 576 nm) (bottom) at RT.

Emission spectra

(a)

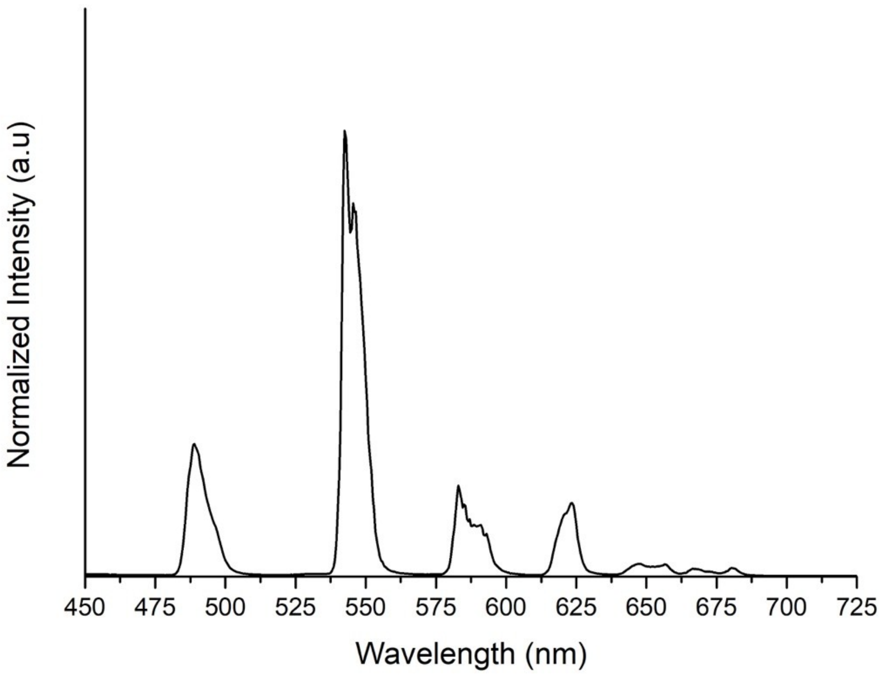

(b)

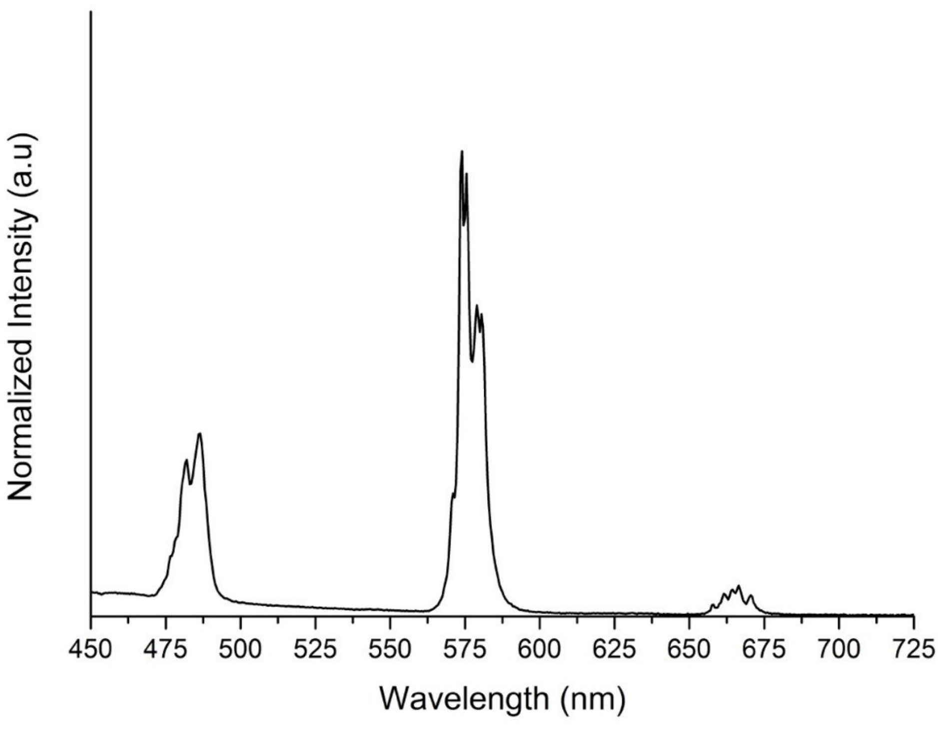

Figure S2: Emission spectra (λ_{ex} = 350 nm) of **HL3-Tb** (a) and **HL3-Dy** (b) at 77K.

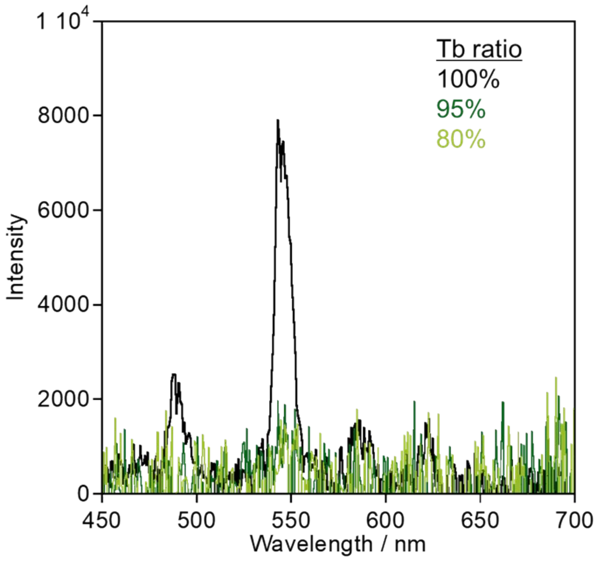

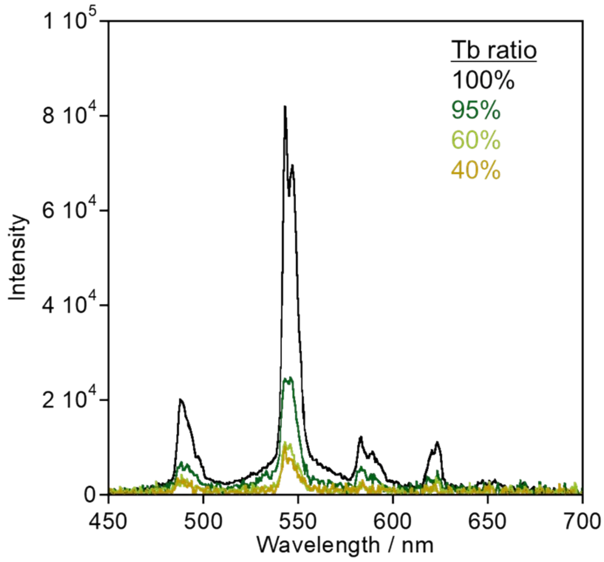

Figure S3: Luminescence spectra observed with absolute luminescence quantum yields spectroscopy, C9920-02 (λ_{ex} = 350 nm) of **HL3**-**Tb1-x Dy** at (a) rt) and (b) 77K.

Table S2: Lifetimes and fit parameters (amplitude; λ_{ex} = 340 nm, λ_{em} = 543 and 574 nm) of f-f electron transitions for **HL3-Tb$_{1-x}$Dy$_x$** solid solutions at room temperature.

Compound	λ_m (nm)	τ_1 (ms)	A_1	τ_2 (ms)	A_2	R
HL3-Tb	543	0.866	100%			1.17
HL3-Tb$_{0.94}$Dy$_{0.06}$	543	0.803	100%			1.31
HL3-Tb$_{0.67}$Dy$_{0.33}$	543	0.470	44.5%	1.096	55.5%	1.24
	574	0.011	99.5%	0.575	0.5%	1.03
HL3-Tb$_{0.42}$Dy$_{0.58}$	543	0.379	42.2%	0.912	57.8%	1.15
	574	0.016	97.6%	0.615	2.4%	1.11
HL3-Tb$_{0.20}$Dy$_{0.80}$	543	0.378	41.2%	0.932	58.8%	1.19
	574	0.022	91.3%	0.401	8.7%	1.15
HL3-Tb$_{0.07}$Dy$_{0.93}$	543	0.335	39.1%	0.857	60.9%	1.04
	574	0.030	94.9%	0.560	5.1%	1.05
HL3-Dy	574	n.d.				

[a] due to apparatus

Table S3: Lifetimes and fit parameters (amplitude; λ_{ex} = 340 nm, λ_{em} = 543 and 574 nm) for of f-f electon transitions for **HL3-Tb$_{1-x}$Dy$_x$** solid solutions at 77K.

Compound	λ_{mon} (nm)	τ_1 (ms)	A_1	τ_2 (ms)	A_2	R
HL3-Tb	543	0.916	100%			1.21
HL3-Tb$_{0.94}$Dy$_{0.06}$	543	0.878	100%			1.22
HL3-Tb$_{0.67}$Dy$_{0.33}$	543	0.894	76.0%	1.571	24.0%	1.15
	574	0.012	99.1%	1.012	0.9%	1.02
HL3-Tb$_{0.42}$Dy$_{0.58}$	543	0.782	75.4%	1.200	24.6%	1.04
	574	0.008	99.1%	0.870	0.9%	1.32
HL3-Tb$_{0.20}$Dy$_{0.80}$	543	0.740	42.7%	1.091	57.3%	1.07
	574	0.083	41.8%	0.915	58.2%	1.01
HL3-Tb$_{0.07}$Dy$_{0.93}$	543	0.882	97.0%	1.986	3.0%	1.01
	574	n.d.				
HL3-Dy	574	n.d.				

[a] due to apparatus

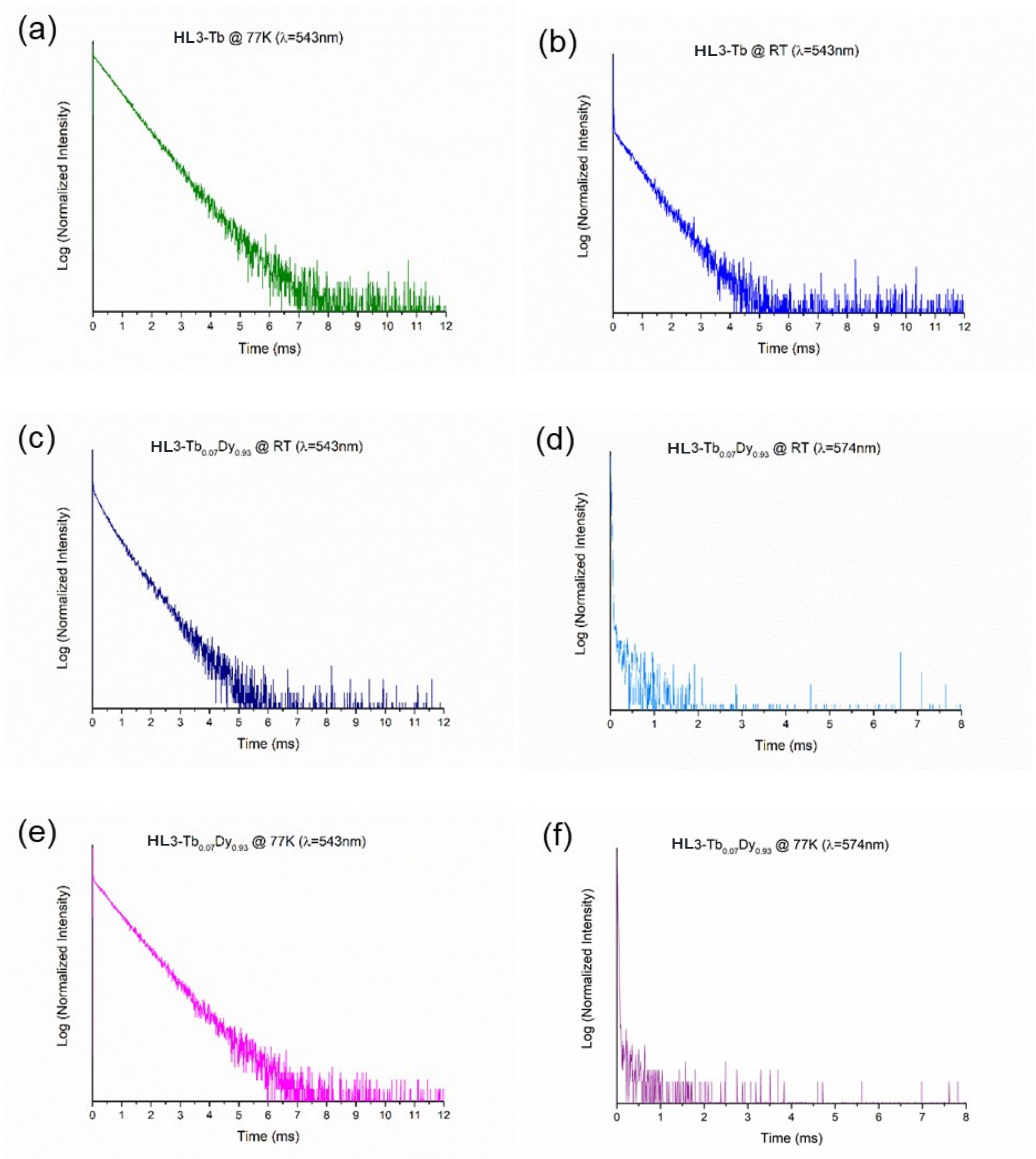

Figure S4: Luminescence decay curves for **HL3**-**Tb**$_{1-x}$**Dy**$_{x}$ solid solutions (λ_{ex}: 340 nm).

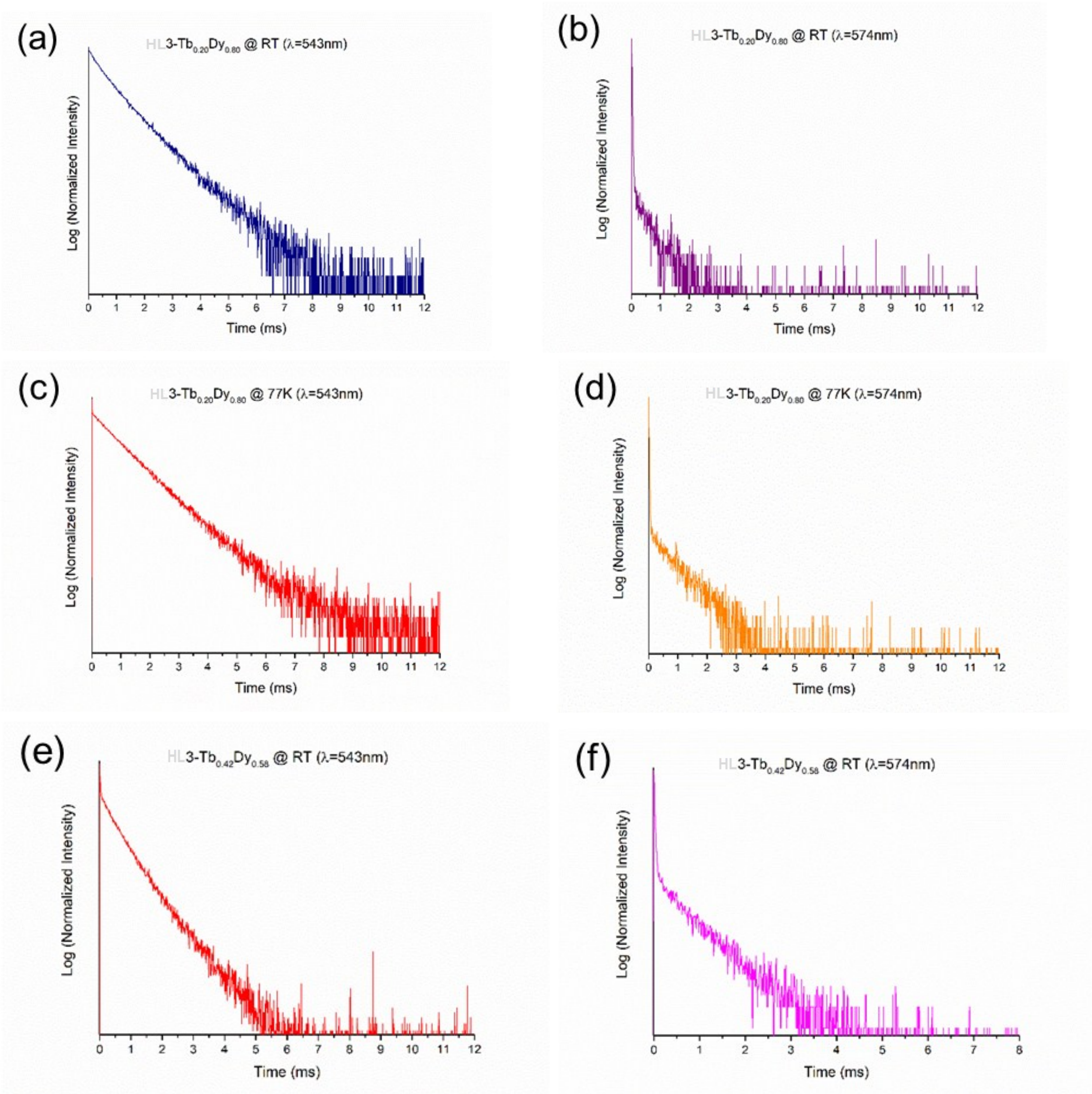

Figure S5: Luminescence decay curves for **HL3-Tb**$_{1-x}$**Dy**$_{x}$ solid solutions (λ_{ex}: 340 nm).

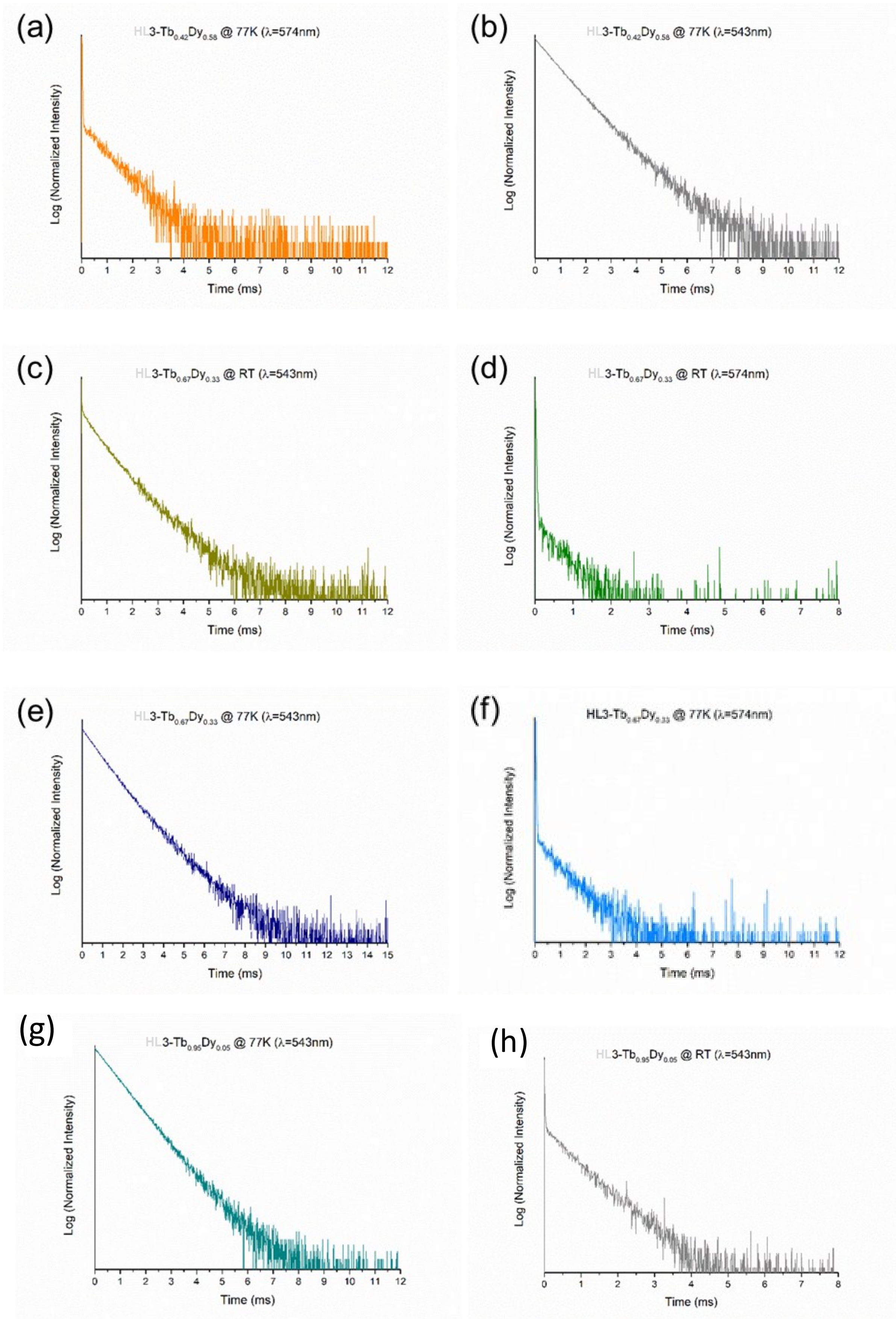

Figure S6: Luminescence decay curves for **HL3-Tb**$_{1-x}$**Dy**$_x$ solid solutions (λ_{ex}: 340 nm).

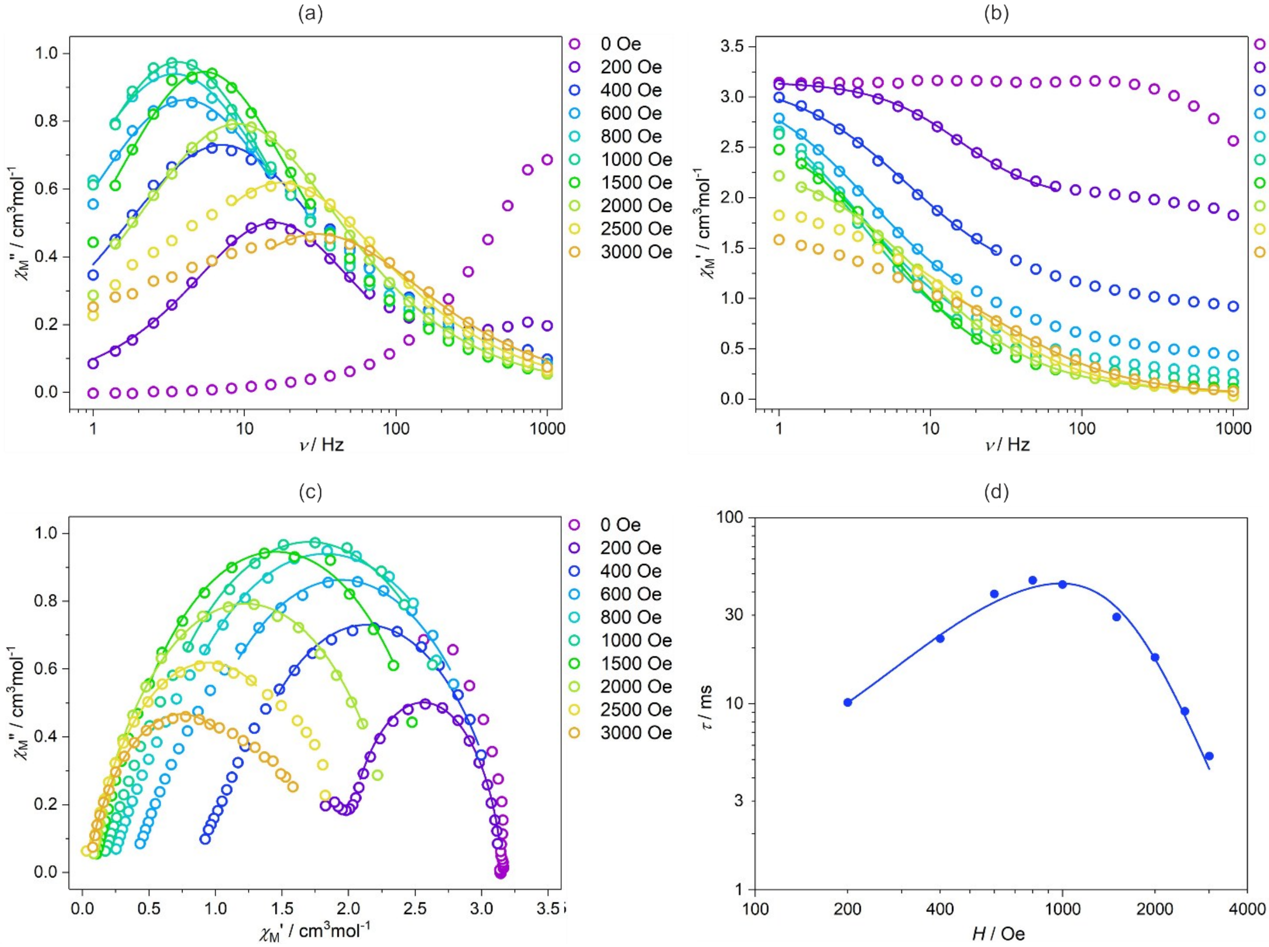

Figure S7. Complete magnetic-field-variable alternate-current (*ac*) magnetic susceptibility characteristics of **HL3-Dy** at T = 1.8 K, under H_{ac} = 1 Oe, and their analysis: frequency dependences of the out-of-phase susceptibility, χ_M'' (*a*), and the in-phase susceptibility, χ_M' (*b*) at various indicated *dc* external magnetic fields, together with the related Argand plots (*c*), and the field dependence of the relaxation time, τ (*d*). Both field and relaxation time were presented in (*d*) in the logarithmic scale. Coloured solid curves in (*a*), (*b*), and (*c*) represent the best fits following the generalized Debye model for a single relaxation process.

The solid line in (*d*) shows the best fit taking into account quantum tunnelling of magnetization, and the direct process, in the range of 200–2000 Oe. The τ versus H_{dc} dependence was fitted using the equation (e1):

$$\tau^{-1} = ATH^4 + \frac{a(1 + c^2H^2)}{(1 + bH^2)} \qquad \text{(e1)}$$

where the first term represented by the *A* parameter is related to a field-induced direct process, while the second term represented by three parameters (*a*, *b* and *c*) is showing the contribution from quantum tunnelling of magnetization. Following the equation, the best-fit parameters are: A = 1.43(5)·10^{-12} $s^{-1}K^{-1}Oe^{-4}$, a = 274(28) s^{-1}, b = 5.3(8)·10^{-5} Oe^{-2}, and c = 1.7(3)·10^{-3} Oe^{-1}.

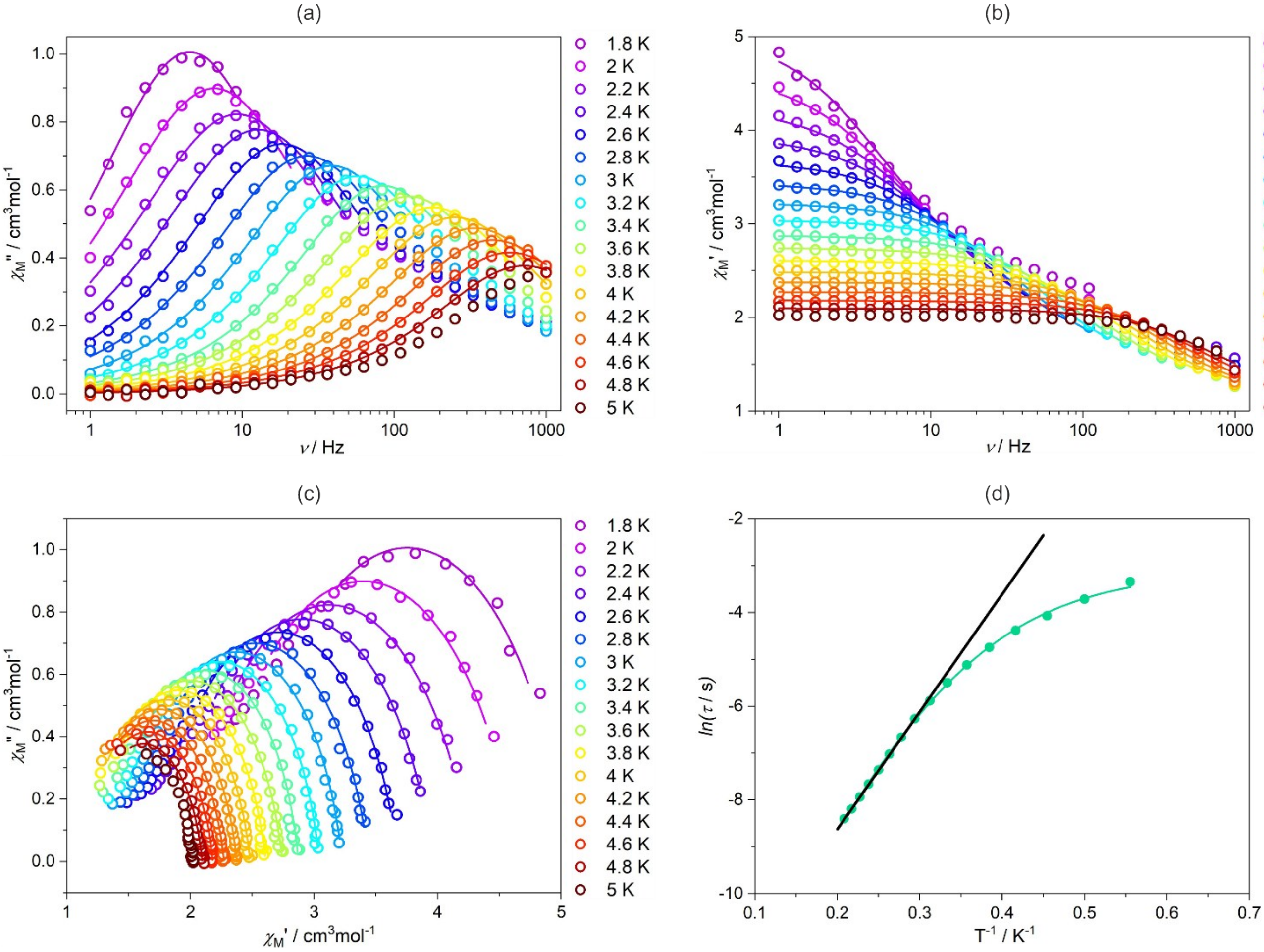

Figure S8. Complete temperature-variable alternate-current (ac) magnetic susceptibility characteristics of **HL3-Dy** under Hac = 1 Oe, Hdc = 1000 Oe, and their analysis: frequency dependences of the out-of-phase susceptibility, χ_M'' (a), and the in-phase susceptibility, χ_M' (b) at various indicated temperatures, together with the related Argand plots (c), and the temperature dependence of the relaxation time, τ (d). Coloured solid curves in (a), (b), and (c) represent the best fits using the generalized Debye model for a single relaxation process.

The solid black line in (d) represents the linear fitting following the Arrhenius law ($\ln\tau = \ln\tau_0 + (U_{eff}/k_B)\cdot T^{-1}$) in the range of 3.4–4.8 K extrapolated towards lower temperatures. The solid green line in (d) shows the best fit taking into account Orbach and Raman relaxation processes, together with a field-induced direct process and quantum tunnelling of magnetization (QTM), in the range of 1.8–4.8 K. Therefore, we followed the equation (e2):

$$\tau^{-1} = \tau_0^{-1} exp(-U_{eff}/k_B T) + B_{Raman}T^n + \frac{a(1+c^2H^2)}{(1+bH^2)} + ATH^4 \quad \text{(e2)}$$

where the first term with two fitting parameters (τ_0, U_{eff}/k_B) represents the Orbach thermal relaxation, the second term indicates the Raman process, the third term shows contribution from the QTM effect, while the last originates from ta field-induced direct process. Parameters extracted from the field-dependence of relaxation times at 1.8 K (*A*, *a*, *b*, *c*) were taken as constants to avoid over-parameterization. The best-fit parameters are: U_{eff}/k_B = 31(3) K, τ_0 = 1.2(7)·10^{-6} s, B_{Raman} = 0.27(1) $s^{-1}K^{-n}$ and n = 6.0(3).

Comment to Figures S7 and S8

For the fitting of the frequency dependences of χ' and χ'' contributions to the *ac* magnetic susceptibility, and the related Argand $\chi''(\chi')$ plots (Figures S7 and S8), the following equations (e3 and e4) of the generalized Debye model for a single relaxation process were used:

$$\chi'(\omega) = \chi_S + (\chi_T - \chi_S)\frac{1 + (\omega\tau)^{1-\alpha}\sin\left(\pi\alpha/2\right)}{1 + 2(\omega\tau)^{1-\alpha}\sin\left(\pi\alpha/2\right) + (\omega\tau)^{2(1-\alpha)}} \quad \text{(e3)}$$

$$\chi''(\omega) = (\chi_T - \chi_S)\frac{(\omega\tau)^{1-\alpha}\cos\left(\pi\alpha/2\right)}{1 + 2(\omega\tau)^{1-\alpha}\sin\left(\pi\alpha/2\right) + (\omega\tau)^{2(1-\alpha)}} \quad \text{(e4)}$$

where

χ_S = the adiabatic susceptibility (at infinitely high frequency of *ac* field),
χ_T = the isothermal susceptibility (at infinitely low frequency of *ac* field),
τ = the relaxation time,
α = the distribution (Cole-Cole) parameter,
and ω is an angular frequency, that is $\omega = 2\pi v$, with v being for the linear frequency in [Hz] units.

The results of the fittings according to the Debye model for a single relaxation process for **1** are shown in Figures S7 (*a*–*c*) and S8 (*a*–*c*). The resulting relaxation times (τ) were plotted against applied *dc* field at T = 1.8 K (Figure S7 d) and against temperature under the applied *dc* field of 1000 Oe (Figure S7 d).